Spectrochimica Acta Part A 93 (2012) 106–115

Contents lists available at SciVerse ScienceDirect

Spectrochimica Acta Part A: Molecular and Biomolecular Spectroscopy

journal homepage: www.elsevier.com/locate/saa

Crystal structure, spectroscopic investigations and density functional studies of 4-(4-methoxyphenethyl)-5-benzyl-2H-1,2,4-triazol-3(4H)-one monohydrate

Yavuz Köysal[a], Hasan Tanak[b,*]

[a] Yeşilyurt Demir-Çelik Vocational School, Ondokuz Mayıs University, Samsun, Turkey
[b] Department of Physics, Faculty of Arts and Sciences, Amasya University, 05100, Amasya, Turkey

ARTICLE INFO

Article history:
Received 4 November 2011
Received in revised form 22 January 2012
Accepted 14 February 2012

Keywords:
1,2,4-Triazole
Density functional theory
FT-IR
Non-linear optics
Molecular electrostatic potential

ABSTRACT

The triazol compound 4-(4-methoxyphenethyl)-5-benzyl-2H-1,2,4-triazol-3(4H)-one monohydrate (**I**) has been synthesized and characterized by ^{1}H NMR, ^{13}C NMR, IR, and X-ray single-crystal determination. The molecular geometry, vibrational frequencies and gauge including atomic orbital (GIAO) ^{1}H and ^{13}C NMR chemical shift values of (**I**) in the ground state have been calculated using the density functional method (B3LYP) with the 6−31G(d) basis set. The calculated results show that the optimized geometry can well reproduce the crystal structure, and the theoretical vibrational frequencies and chemical shift values show good agreement with experimental values. The energetic behavior of (**I**) in solvent media was examined using the B3LYP method with the 6−31G(d) basis set by applying the Onsager and the polarizable continuum model (PCM). The predicted non-linear optical properties of (**I**) are greater than ones of urea. In addition, DFT calculations of molecular electrostatic potentials, frontier molecular orbitals and thermodynamic properties of (**I**) were carried out at the B3LYP/6−31G(d) level of theory.

1. Introduction

The chemistry and structure of heterocyclic compounds has an interesting field of study for a long time. The synthesis of 1,2,4-triazoles and investigation of their chemical and biological behavior have gained more importance in recent decades for biological, medicinal and agricultural reasons. 1,2,4-triazole compounds possess important pharmacological activities such as antifungal and antiviral activities. Examples of such compounds bearing the 1,2,4-triazole residues are fluconazole [1], the powerful azole antifungal agent as well as the potent antiviral N-nucleoside ribavirin [2]. Furthermore, various 1,2,4-triazole derivatives have been reported as fungicidal, insecticidal, antimicrobial as well as anticonvulsants, antidepressants, and plant growth regular anticoagulants [3–8]. It is known that 1,2,4-triazol moieties interact strongly with heme iron, and aromatic substituents on the triazoles are very effective for interacting with the active site of aromatase. Furthermore, it was reported that compounds having triazole moieties such as Vorozole, Anastrozole and Letrozole appear to be very effective aromatase inhibitors very useful for preventing breast cancer.

The literature concerning the 1,2,4-triazole is rich and the papers published cover such subjects as crystal structure determination [9–11], ab initio and DFT calculations on the tautomerism and protonation sites [12–14], vibrational characteristics and photochemical transformations [15–18] and thermal decomposition products [19,20]. Many reports have appeared on the synthesis and characterization of novel triazole containing organic [21,22] or metal coordination compounds [23,24] including spin-crossover materials [25,26].

In recent years, density functional theory (DFT) has been extensively used in theoretical modeling. The development of better exchange–correlation functionals has made it possible to calculate many molecular properties with comparable accuracies to traditionally correlated ab initio methods, with more favorable computational costs [27]. Literature survey has revealed that the DFT has a great accuracy in reproducing the experimental values in geometry, dipole moment, vibrational frequency, etc. [28–32].

The aim of this study is to investigate the energetic and structural properties of the 1,2,4-triazole compound, 4-(4-methoxyphenethyl)-5-benzyl-2H-1,2,4-triazol-3(4H)-one monohydrate (Fig. 1), using density functional theory calculations. In this study, the optimized geometry, vibrational spectra and assignments, statistical thermodynamic parameters, natural bond orbital analysis and nonlinear optical properties of (**I**) have been studied. These calculations are valuable for providing insight into molecular properties of 1,2,4-triazole compounds.

2. Experimental and computational methods

2.1. Synthesis

Ethyl-2-(1-ethoxy-2-phenylethylidene)hydrazine carboxylate (10 mmol) together with 2-(4-methoxyphenyl)ethylamine

---

* Corresponding author. Tel.: +90 358 218 01 60; fax: +90 358 218 01 04.
E-mail address: hasantanak@gmail.com (H. Tanak).

1386-1425/$ – see front matter © 2012 Elsevier B.V. All rights reserved.
doi:10.1016/j.saa.2012.02.054

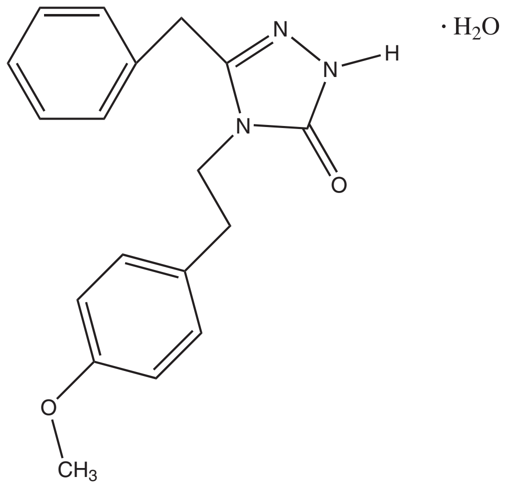

Fig. 1. Chemical diagram of 4-(4-methoxyphenethyl)-5-benzyl-2H-1,2,4-triazol-3(4H)-one monohydrate.

(10 mmol) were heated without solvent in a sealed tube for 2 h at 150–160 °C. Then, the mixture was cooled to r.t. and a solid crude formed. The crude product was recrystallized using ethyl acetate/petroleum ether (3:1) to afford the desired compound. Yield: 196 mg (88%). Colorless crystals. M.P. 385 K.

2.2. Physical measurements

The melting point was determined using a Gallenkamp melting point apparatus. The IR spectrum of (**I**) was recorded in the range 4000–400 cm^{-1} using a Perkin-Elmer 1600 series FTIR spectrophotometer with KBr pellets. The spectrum was recorded at room temperature with scanning speed of 10 cm^{-1} min^{-1} and the spectral resolution of 4.0 cm^{-1}. The ^1H and ^{13}C nuclear magnetic resonance spectra were recorded on a Varian-Mercury 200 MHz spectrometer using TMS as standard and $CDCl_3$ as solvent.

2.3. Crystal structure determination

A block of single crystal with dimensions 0.80 mm × 0.57 mm × 0.41 mm was mounted on goniometer and data collection was performed on a STOE IPDS II [33] diffractometer by the ω scan technique using graphite-monochromatic MoK_α radiation ($\lambda = 0.71073$ Å) at 296 K. The intensity symmetries indicate the monoclinic $P2_1/c$ space group. A total of reflections 11,228 (3501 unique) were performed within 2θ range 1.27° and 26.75°. Correction for absorption ($\mu = 0.091$), by comparison of the intensities of equivalent reflections, was applied using X-RED software [33] and cell parameters were determined by using X-AREA software [33]. The initial partial solution obtained by direct methods as implemented in the program SHELXS-97 [34] was expanded and refined by means of the program SHELXL-97 [34]. The program ORTEP-3 for windows [35] has been used in the preparation of the figures. All non-hydrogen atoms were refined anisotropically. The refinement carried out by full matrix least squares method on the positional and anisotropic temperature parameters of non-hydrogen atoms corresponding to 229 crystallographic parameters. All the H atoms were located geometrically and refined using a riding model, except for H22, H33 and H44, fixing the bond lengths at 0.93 Å, 0.96 Å and 0.97 Å for CH, CH_3 and CH_2, respectively. The structure was refined to $R_{int} = 0.0592$ with 2637 observed reflections by the condition of $I > 2\sigma(I)$ threshold. Details of the data collection conditions and the parameters of refinement process are given in Table 1.

Table 1
Crystal data and structure refinement parameters for the title compound.

Chemical formula	$C_{18}H_{21}N_3O_3$
Formula weight	327.38
Temperature (K)	296
Wavelength (Å)	0.71073
Crystal system	Monoclinic
Space group	$P2_1/c$
Unit cell parameters	
a, b, c (Å)	6.7971(3), 32.0286(16), 9.1496(4)
α, β, γ (°)	90.00, 124.244(3), 90.00
Volume (Å^3)	1646.59 (13)
Z	4
Calculated density (Mg/m^3)	1.321
μ (mm^{-1})	0.09
Absorption correction	Integration (X-RED32)
F_{000}	696
Crystal size (mm)	0.700 × 0.483 × 0.270
Index ranges	$-8 \le h \le 8$, $-40 \le k \le 40$, $-11 \le l \le 11$
Diffractometer/measurement method	STOE IPDS II/rotation (ω scan)
Theta range for data collection (°)	$1.3 \le \theta \le 26.8$
Measured reflections	11,228
Independent/observed reflections	3501/2637
R_{int}	0.059
Refinement method	Full-matrix least-squares on F^2
Data/restraints/parameters	2637/0/229
Goodness-of-fit on F^2	1.01
R indices [$I > 2\sigma(I)$]	0.051
R indices (all data)	0.066
Weighting scheme	$w = 1/[\sigma^2(F_o{}^2) + (0.0756P)^2]$; $P = (F_o{}^2 + 2F_c{}^2)/3$
$\Delta\rho_{max}$, $\Delta\rho_{min}$ (e/Å^3)	0.29, −0.49

2.4. Computational methods

The molecular geometry was taken directly from the X-ray diffraction experimental result without any constraints. In the next step, the DFT calculations with a hybrid functional B3LYP (Becke's Three parameter hybrid functional using the LYP correlation functional) with the 6−31G(d) basis set using the Berny method [36,37] were performed with the Gaussian 03W software package [38]. The harmonic vibrational frequencies were calculated at the same level of theory for the optimized structure and the obtained frequencies were scaled by 0.9613 [39]. Vibrational band assignments were made using the Gauss-View molecular visualization program [40]. In order to evaluate the energetic and atomic charge behavior of (**I**) in solvent media, we also carried out optimization calculations in five solvents ($\varepsilon = 78.39$, H_2O; $\varepsilon = 46.7$, DMSO; $\varepsilon = 24.55$, C_2H_5OH; $\varepsilon = 10.36$, CH_2ClCH_2Cl; $\varepsilon = 4.9$, $CHCl_3$) at the B3LYP/6−31G(d) level using the Onsager [41] and Polarizable Continuum Model (PCM) [42–45] methods. To investigate the reactive sites of (**I**) the molecular electrostatic potentials were evaluated using B3LYP/6−31G(d) method. Molecular electrostatic potential, $V(\mathbf{r})$, at a given point $\mathbf{r}(x, y, z)$ in the vicinity of a molecule, is defined in terms of the interaction energy between the electrical charge generated from the molecule's electrons and nuclei and a positive test charge (a proton) located at $\mathbf{r}$. For the system studied the $V(\mathbf{r})$ values were calculated as described previously using the equation [46],

$$V(\mathbf{r}) = \sum_{A} \frac{Z_A}{|\mathbf{R}_A - \mathbf{r}|} - \int \frac{\rho(\mathbf{r}')}{|\mathbf{r}' - \mathbf{r}|} d\mathbf{r}' \qquad (1)$$

where Z_A is the charge of nucleus A, located at $\mathbf{R}_A$, $\rho(\mathbf{r}')$ is the electronic density function of the molecule, and $\mathbf{r}'$ is the dummy integration variable. The mean linear polarizability and mean first hyperpolarizability properties of (**I**) were obtained from molecular polarizabilities based on theoretical calculations. The NBO analysis was performed at the B3LYP/6−31G(d) level by means of the NBO 3.1 program within the Gaussian 03W package [47]. The

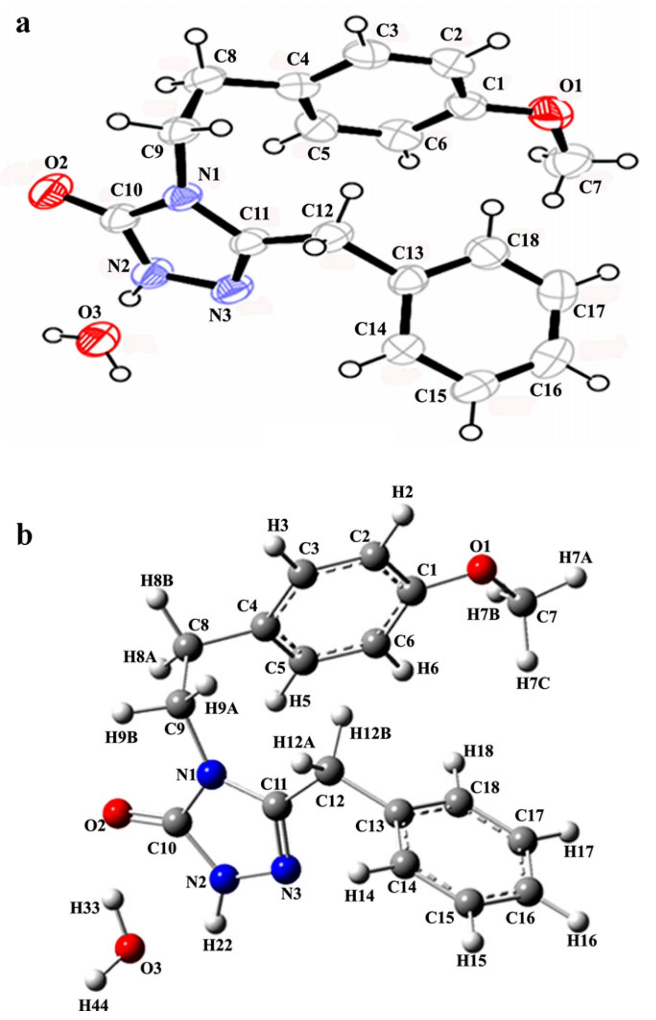

Fig. 2. (a) Ortep-3 diagram of the title compound. Displacement ellipsoids are drawn at the 30% probability level and H atoms are shown as small spheres of arbitrary radii. (b) The theoretical geometric structure of the title compound (B3LYP/6−31G(d) level).

thermodynamic properties of (**I**) at different temperatures were calculated on the basis of vibrational analyses.

3. Results and discussion

3.1. Description of the crystal structure

The crystal structure of (**I**) is monoclinic and space group $P2_1/c$. The molecular structure of (**I**) shown in Fig. 2a is not planar but each ring system is planar individually. In the molecule of (**I**), $C_{18}H_{21}N_3O_3$, contains the 1,2,4-triazol ring, the methoxyphenethyl ring, benzyl ring. Triazol ring is oriented with respect to the 5-benzyl and 4-methoxyphenethyl rings at dihedral angles of 55.01(2)° and 35.88(2)°, respectively. Triazol ring system is almost planar with the maximum deviation of 0.0015(1) Å for atom C11. The molecular geometry of the triazol ring is in agreement with the values of structure 4-(3-Methoxyphenyl)-3-[2-(4-methoxyphenyl)ethyl]-1H-1,2,4-triazol-5(4H)-one [48].

In the molecule of (**I**), the bond lengths and angles are within normal ranges and they are comparable with those related structure [49]. Title compound, $C_{18}H_{21}N_3O_3$, containing the triazol ring display the characteristic features of 1,2,4-triazol derivatives.

The interatomic distances within the triazole ring of (**I**) are not equal. The N3═C11 is double bond and shorter than the conjugated C10—N1 and C11—N1 bonds. The molecular geometry of the triazole ring is in agreement values with the structure 5-benzyl-4-(3,4-dimethoxyphenethyl)-2H-1,2,4-triazol-3(4H)-one [50]. The torsion angle around the (N1—C9—C8—C4) is −64.66(2)°.

Table 2
Hydrogen-bond geometry (Å,°).

D—H···A	D—H	H···A	D···A	D—H···A
O3—H33···O2^{i}	0.90 (2)	1.87 (2)	2.7601 (16)	169.9 (19)
O3—H44···O2^{ii}	0.88 (3)	1.94 (3)	2.8233 (16)	174 (2)
N2—H22···O3^{iii}	0.93 (2)	1.92 (2)	2.8386 (16)	168.8 (17)

Symmetry codes: (i) $-x+1, -y+1, -z$; (ii) $x+1, y, z$; (iii) $x, y, -1+z$.

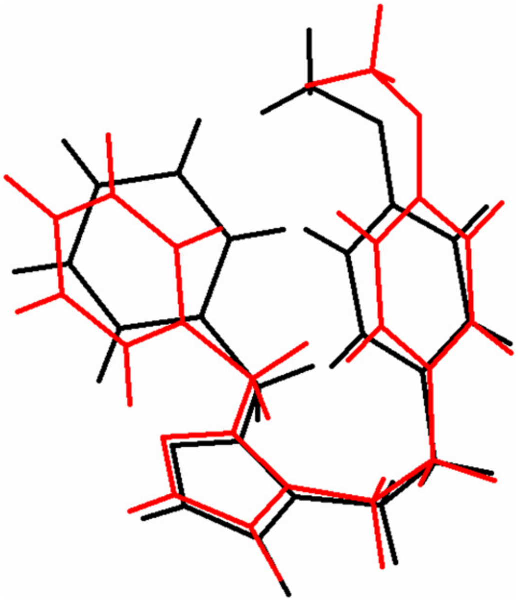

Fig. 3. Atom-by-atom superimposition of the structure calculated (red) over the X-ray structure (black) for the title compound. (For interpretation of the references to color in this figure legend, the reader is referred to the web version of the article.)

Structurally, the organic molecule forms O—H···O and N—H···O types intermolecular hydrogen bonds (Table 2). The intermolecular contacts are O3—H33···O2^{i} and O3—H44···O2^{ii} where atom O2 accepts hydrogen bonds from O—H donors [symmetry codes: (**I**) $-x+1, -y+1, -z$; (ii) $x+1, +y, +z$]. The H atoms of the water molecule are engaged in hydrogen bonding with O2 atom of the attached triazol system which link the molecules into discrete pairs across crystallographic centers of symmetry. There is also short intermolecular contact is namely N2—H22···O3 [symmetry code: (iii) $x, y, -1+z$].

3.2. Optimized geometry

The optimized parameters (bond lengths, bond angles, and dihedral angles) of (**I**) were obtained using the B3LYP/6−31G(d) method. The atomic numbering scheme of the theoretical geometric structure is shown in Fig. 2b. Calculated geometric parameters are listed in Table 3 along with the experimental data. When the X-ray structure of (**I**) is compared with its optimized counterparts (see Fig. 3), slight conformational discrepancies are observed between them. We note that the experimental results are for the solid phase and the theoretical calculations are for the gas phase. In the solid state, the existence of a crystal field along with the intermolecular interactions connects the molecules together, which results in the differences in bond parameters between the calculated and experimental values. The most notable discrepancies are found in the orientation of the benzyl ring of (**I**), which is defined by torsion

Table 3
Selected molecular structure parameters.

Parameters	Experimental	B3LYP/6−31G(d)
Bond lengths (Å)		
O2—C10	1.2413(17)	1.238
N1—C10	1.3738(17)	1.393
N1—C11	1.3790(17)	1.388
N1—C9	1.4605(16)	1.457
N2—C10	1.3388(18)	1.363
N2—N3	1.3826(17)	1.376
C11—N3	1.2960(17)	1.303
C11—C12	1.4914(19)	1.503
C9—C8	1.523(2)	1.544
C4—C5	1.386(2)	1.397
C4—C3	1.391(2)	1.406
C4—C8	1.505(2)	1.512
O1—C1	1.374(2)	1.364
O1—C7	1.417(2)	1.419
C13—C18	1.382(2)	1.399
C13—C14	1.385(2)	1.398
C13—C12	1.509(2)	1.515
C14—C15	1.385(2)	1.395
C5—C6	1.386(2)	1.398
C18—C17	1.388(2)	1.394
C1—C6	1.382(2)	1.399
C1—C2	1.384(2)	1.403
C3—C2	1.378(2)	1.388
C15—C16	1.368(3)	1.395
C16—C17	1.367(3)	1.396
Bond angles (°)		
C10—N1—C11	107.49(10)	107.65
C10—N1—C9	122.63(11)	122.08
C11—N1—C9	129.23(11)	130.23
C10—N2—N3	112.53(11)	113.45
N3—C11—N1	111.22(12)	111.45
N3—C11—C12	126.31(12)	125.25
N1—C11—C12	122.36(11)	123.27
C11—N3—N2	104.48(11)	104.51
N1—C9—C8	111.64(11)	113.23
C5—C4—C3	117.15(14)	117.59
C5—C4—C8	121.66(13)	121.34
C3—C4—C8	121.11(13)	121.04
C4—C8—C9	113.11(12)	114.20
C1—O1—C7	118.18(13)	118.23
C18—C13—C14	118.14(14)	118.86
C18—C13—C12	119.99(14)	120.37
C14—C13—C12	121.81(14)	120.76
C11—C12—C13	115.53(11)	113.69
C13—C14—C15	120.69(15)	120.69
O2—C10—N2	129.36(13)	129.81
O2—C10—N1	126.36(12)	127.26
N2—C10—N1	104.28(11)	102.92
C4—C5—C6	122.09(14)	121.81
C13—C18—C17	120.79(15)	120.60
O1—C1—C6	125.02(14)	124.87
O1—C1—C2	115.40(14)	115.72
C6—C1—C2	119.57(14)	119.39
C2—C3—C4	121.60(14)	121.50
C16—C15—C14	120.47(16)	120.05
C3—C2—C1	120.13(14)	120.07
C17—C16—C15	119.61(15)	119.64
C1—C6—C5	119.42(14)	119.61
C16—C17—C18	120.29(16)	120.13
Torsion angles (°)		
C3—C4—C8—C9	−88.91(17)	−83.44
C5—C4—C8—C9	87.64(17)	95.049
N1—C9—C8—C4	−64.66(15)	−64.25
C11—N1—C9—C8	95.36(17)	102.31
C10—N1—C9—C8	−74.24(17)	−75.41
N1—C11—C12—C13	−165.67(13)	−176.85
N3—C11—C12—C13	18.4(2)	4.51
C14—C13—C12—C11	−65.57(19)	−92.14
C18—C13—C12—C11	117.29(16)	88.21
C7—O1—C1—C2	168.83(15)	−179.62
C7—O1—C1—C6	−10.2(2)	−0.039

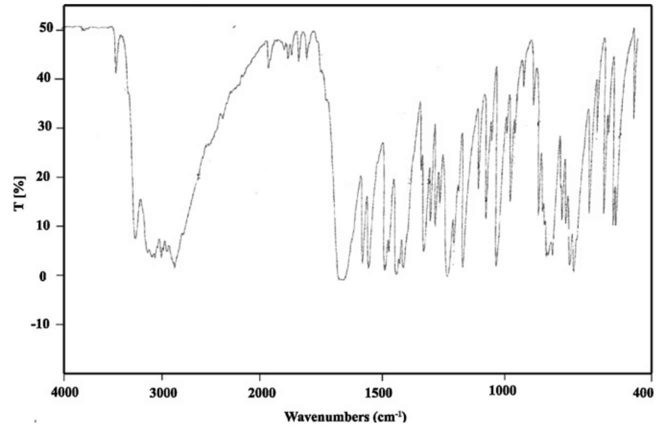

Fig. 4. FT-IR spectrum of the title compound.

angles C11—C12—C13—C14 [−65.57(19)°] and C11—C12—C13—C18 [117.29(16)°]. These torsion angles have been calculated at −92.14 and 88.21° for B3LYP/6−31G(d) level. Another difference in the optimized structure is observed in the relative orientation of the triazole and methoxyphenethyl rings. The dihedral angle between the triazole and methoxyphenethyl rings is 35.88(2)° for X-ray, whereas the dihedral angle has been calculated as 48.31° for B3LYP.

A logical method for globally comparing the structures obtained with the theoretical calculations is by superimposing the molecular skeleton with that obtained from X-ray diffraction, giving a RMSE of 0.797 Å for B3LYP/6−31G(d) (Fig. 3). This RMSE value is quite large. This magnitude of RMSE can be explained by the fact that the intermolecular Coulombic interaction with the neighboring molecules are absent in gas phase, whereas the experimental result corresponds to interacting molecules in the crystal lattice [28].

3.3. *IR spectroscopy*

Harmonic vibrational frequencies of (**I**) were calculated using the DFT/B3LYP method with 6−31G(d) basis set. The vibrational band assignments were made using the Gauss-View molecular visualization program. In order to facilitate assignment of the observed peaks, we have analyzed the vibrational frequencies and compared our calculation for (**I**) with the experimental results (Table 4). The agreement between the experimental and calculated frequencies is quite good in general.

The FT-IR spectra of (**I**) were recorded in the 4000–400 cm^{-1} region using KBr pellets on a Schmadzu FT-IR 8900 spectrophotometer and given in Fig. 4. The OH group vibrations are likely to be most sensitive to the environment, so they show pronounced shifts in the spectra of the hydrogen-bonded species. The non-hydrogen-bonded or a free hydroxyl group absorb strongly in the 3550–3700 cm^{-1} region [62]. Intra- and intermolecular hydrogen bonding if present in the molecule would reduce the O—H stretching band to 3000–3550 cm^{-1} region [51]. The IR spectra of (**I**) has got an intense and relatively sharp band with a maximum at 3370 cm^{-1} was assigned to the stretching vibrations of the sub group in the very weak intermolecular O—H···O hydrogen bonds formed between the water molecule and the O atom of carbonyl group. This band has been calculated at 3647 cm^{-1} for B3LYP level. In the literature, some N—H stretching modes observed for the different substituent-triazole ring are 3383 cm^{-1} [52] and 3417 cm^{-1} [53] as experimentally. In our study, the N—H stretching mode was observed at 3170 cm^{-1} which has a red shift and the cause of this shift is the intermolecular N2—H22···O3 hydrogen bonding. The red shifting is further enhanced by the reduction in the N—H bond order values, occurring due to donor–acceptor interaction [54].

Table 4
Comparison of the experimental and calculated vibrational frequencies (cm^{-1}).

Assignments[a]	Experimental IR with KBr	B3LYP/6−31G(d)
ν(O—H)	3370	3647
ν(N—H)	3170	3404
ν_s(C—H) of R2		3090
ν_s(C—H) of R1		3084
ν_{as}(C—H) of R1		3074
ν_{as}(C—H) of R2	3060	3064
ν_{as}(C—H) of R1		3056
ν_{as}(C—H) of R1		3053
ν_{as}(C—H) of R2		3049
ν_s(C—H_3)		3037
ν_{as}(C—H_2)	3021	3014
ν_{as}(C—H_2)		2987
ν_{as}(C—H_3)	2947	2966
ν_s(C—H_2)		2963
ν_s(C—H_2)		2934
ν_s(C—H_2)		2913
ν_s(C—H_3)		2909
ν(C=O)	1692	1715
ν(C=C)	1609	1609
ν(C=C)		1603
ν(C=N) + β(NCN)	1582	1572
ν(C=C)		1567
γ(C—H) of R2 + ω(CH_3)	1513	1506
γ(C—H) of R1	1496	1490
ω(C—H_3)	1463	1475
ν(C—N) of triazole + ν(C—C)	1433	1413
γ(N—H)	1366	1358
β(C—H_2) + $\tau_{aliphatic}$ (HCCC)	1349	1341
ν(C—C) of R2 + β(C—H_2)	1322	1324
ν(C—C) of R2 + ω(C—H_2)	1302	1311
β(C—H_2) + ω(CH_3)	1284	1295
ν(C—O) + γ(C—C) of R2	1245	1250
ω(C—H_2) + $\tau_{aliphatic}$ (HCNC) + $\tau_{aliphatic}$ (HCCC)	1220	1228
δ(C—H_2) + $\tau_{aliphatic}$ (HCCC)	1181	1161
ν(C—C) of R2 + γ(C—H) of R2 + ω(CH_3)	1119	1102
ν(N—N)	1085	1065
ν(O—C)	1037	1035
ν(C—C) of R1 + β(CCC) of R1	982	980
ω(C—H) of R2 + τ(CCCC) of R2	935	925
ω(C—H) of R1 + ω(C—H) of R1	892	893
ω(C—H) of R2	822	810
ω(C—H) of R2	798	796
β(O—H)	760	772
β(CNN) of triazole + β(O—H)	743	754
τ(HNNC) of triazole	705	709
β(OCN)	643	643
β(CCC) of R1	616	612
τ(CNNC) of triazole + τ(CCCN) of triazole	580	602
β(CCC) + τ(CCCC) of R2 + out of plane (OCCC)	538	547
β(OCN)	527	517
Out of plane (OCCC)	459	456

[a] ν, stretching; γ, rocking; ω, wagging; β, bending; τ, torsion; δ, out of plane bending; s, symmetric; as, asymmetric. Abbreviations: R1; phenyl ring; R2; methoxyphenyl ring.

The theoretically calculated harmonic wavenumber at 3404 cm^{-1} by B3LYP/6−31G(d) shows little deviation on the higher side. These differences of O—H (277 cm^{-1}) and N—H stretching vibrations (234 cm^{-1}) occurred between the results of the experimental and calculations are due to the consideration of the isolated molecules (in gas phase) in the calculational method. Therefore, we can conclude that these differences can be explained by the existence of the intermolecular interactions in molecular structure of (**I**). The aromatic C—H stretching, C—H in-plane bending and C—H out-of-plane bending vibrations appear in 2900–3150 cm^{-1}, 1100–1500 cm^{-1} and 700–1000 cm^{-1} frequency ranges, respectively. The C—H aromatic stretching mode was observed at 3060 cm^{-1} experimentally, and calculated at 3049–3090 cm^{-1} for B3LYP. The bands at 3021 and 2947 cm^{-1} correspond to the asymmetric stretching CH_2 and CH_3 modes, respectively. The C—H in-plane bending vibrations computed at 1506, 1490 and 1102 cm^{-1} by B3LYP/6−31G(d) method shows excellent agreement with FT-IR bands at 1513, 1496 and 1119 cm^{-1}. The bands observed at 935, 892, 822 and 798 cm^{-1} in FT-IR spectra are assigned to ring C—H out-of-plane bending vibration for (**I**).

The stretching C=O vibration gives rise to a band in the infrared experimental spectrum at 1692 cm^{-1}, while the calculated value is predicted 22 cm^{-1} lower, at 1714 cm^{-1}. Triazole (C=N) bond stretching vibration was observed to be 1582 cm^{-1} experimentally, while that have been calculated at 1572 cm^{-1} for B3LYP. The identification of C—N vibrations is a very difficult task, since mixing of several bands is possible in this region. However, the C—N stretching assignments are identified by the animation application of Gauss-View 4.1.2 graphical interface for Gaussian output file. Silverstein et al. [55] assigned C—N stretching absorption in the region 1382–1266 cm^{-1} for aromatic amines. In benzotrizole, the C—N stretchings are found to be present at 1382 and 1307 cm^{-1} [56]. We have predicted the same vibration at 1339 cm^{-1} in 5-benzyl-4-(3,4-dimethoxyphenethyl)-2H-1,2,4-triazol-3(4H)-one [50]. In the present study, a very strong band at 1433 cm^{-1} in FT-IR has been assigned to triazole C—N stretching vibration. These results indicated some band shifts with regard to the different substituent-triazole ring. The theoretically computed value of C—N stretching vibration is defined as 1413 cm^{-1}. The C—O stretching vibrations were observed at 1245 and 1037 cm^{-1} which confirms the presence of methoxy group in the compound. These bands have been calculated at 1250 and 1035 cm^{-1} for B3LYP level.

The benzene ring modes predominantly involve C=C bonds and the vibrational frequency is associated with C=C stretching modes of carbon skeleton [51]. The band observed at 1609 cm^{-1}, which can be attributed to the C=C stretching vibration, were calculated at 1609–1567 cm^{-1} for B3LYP. The bands observed at 538, 616 and 982 cm^{-1} in the FT-IR spectra are ascribed to the vibration modes including the phenyl CCC angle bending. The theoretically computed values of the angles bending vibration modes show good agreement with the experimental values. The other vibrational frequencies can be seen in Table 4.

3.4. NMR spectra

GIAO ^{1}H and ^{13}C chemical shift values (with respect to TMS) were calculated using the B3LYP method with 6−31G(d) basis set and generally compared to the experimental ^{1}H and ^{13}C chemical shift values. The results of this calculation are shown in Table 5.

We have calculated ^{1}H chemical shift values (with respect to TMS) of 9.11–0.54 ppm at B3LYP/6−31G(d) level, whereas the experimental results are observed to be 11.54–2.5 ppm. The OCH_3 protons of (**I**) gave a singlet at 3.72 ppm. This was calculated 3.6–3.98 ppm at B3LYP level. The triplets observed at 3.42 and 3.54 ppm are assigned to C(8)H_2 and C(9)H_2 groups, respectively, that have been calculated at 2.50–3.25 and 3.24–3.93 ppm. The aromatic C—H signals were observed to be 7.26–7.34, 7.17, 6.93 and 6.85 ppm.

In differently substituent 1,2,4-triazole, the ^{1}H chemical shift of N—H were observed to be 11.33–13.56 ppm [57]. The NH hydrogen of the 1,2,4-triazole ring appears at 11.54 ppm, and is determined computationally at 9.11 ppm. The signal assigned to protons of the water molecule is observed at 2.5 ppm. This was calculated 0.54–4.06 ppm at B3LYP level. Because the intermolecular hydrogen bonds in molecular structure of (**I**) are neglected in the calculations, we can say that this difference between experimental and calculated chemical shifts is due to N—H···O and O—H···O intermolecular interactions.

^{13}C NMR spectra of (**I**) show signals at 158.67 and 155.68 ppm due, respectively, to the C10 and C11 atoms of the triazole ring.

Table 5
Theoretical and experimental ^{1}H and ^{13}C isotropic chemical shifts (with respect to TMS, all values in ppm) for the title compound.

Atom	Experimental (ppm) ($CDCl_3$)	Calculated (ppm) B3LYP/6−31G(d)
C1	146.93	150.39
C2	114.57	112.25
C3	129.42	123.28
C4	130.46	123.6
C5	129.42	125.66
C6	114.57	103.43
C7	55.65	52.56
C8	33.80	35.21
C9	42.89	45.67
C10	158.67	146.35
C11	155.68	140.33
C12	31.97	33.37
C13	136.04	126.71
C14	130.41	123.78
C15	129.33	121.15
C16	127.62	120.07
C17	129.33	121.16
C18	130.41	123.93
H2	6.85	6.8
H3	6.93	7.16
H5	6.93	6.86
H6	6.85	6.43
H7A	3.72	3.98
H7B	3.72	3.6
H7C	3.72	3.69
H8A	3.42	3.25
H8B	3.42	2.50
H9A	3.54	3.24
H9B	3.54	3.93
H12A	3.62	2.95
H12B	3.62	2.40
H14	7.17	6.9
H15	7.26–7.34	7.1
H16	7.26–7.34	7.08
H17	7.26–7.34	7.06
H18	7.17	6.49
H22	11.54	9.11
H33	2.50	4.06
H44	2.50	0.54

These signals were calculated at 146.35 and 140.33 ppm, respectively. The chemical shift values of C1 atom bounded OCH_3 group is observed as 146.93 ppm, whereas the corresponding value is 150.39 ppm for B3LYP level. While the C atom of the methoxy group belonging to the benzyl ring is observed at 55.65 ppm, the aliphatic CH_2 (C8, C9, and C12) carbons are observed at 33.80, 42.89 and 31.97 ppm, respectively. The other calculated chemical shift values can be seen in Table 5. As can be seen from Table 5, the theoretical ^{1}H and ^{13}C chemical shift results for (**I**) are generally closer to the experimental ^{1}H and ^{13}C shift data.

3.5. Energetics and dipole moments

In order to evaluate the total energy and dipole moment behavior of (**I**) in solvent media, we carried out calculations in five solvents ($\varepsilon = 78.39$, H_2O; $\varepsilon = 46.7$, DMSO; $\varepsilon = 24.55$, C_2H_5OH; $\varepsilon = 10.36$, CH_2ClCH_2Cl; $\varepsilon = 4.9$, $CHCl_3$). The total energies and dipole moments were calculated in solvent media at the B3LYP/6−31G(d) level using the Onsager and PCM methods and the results are given in Table 6. From this table, we can conclude that the obtained total energy of (**I**) decreases with the increasing polarity of the solvent so that the stability of (**I**) increases. The energy difference between the gas phase and solvent media is shown in Fig. 5 for both methods. As can be seen from Fig. 5, the PCM method provides a more stable structure than Onsager's method (57.87 kJ/mol average). The trend in the total energies is not observed in the dipole moments. The dipole moments calculated by the Onsager method are larger than those for the PCM method in the various solvents, and the dipole moments obtained for the two solvation methods increase with the increasing solvent polarity. Solvent effects improve the charge delocalized in the molecules, therefore, inducing the dipole moments to be raised. Ground-state dipole moment is an important factor in measuring solvent effect, a large ground-state dipole moment gives rise to strong solvent polarity effects [58,59].

Table 6
Total energies and dipole moments of the title compound in different solvents.

Method	ε	Energy (a.u.)	μ (Debye)	ΔE (kJ/mol)
B3LYP	1	−1088.492542	2.949	
Onsager	4.9	−1088.493075	3.850	−1.39939
	10.36	−1088.493220	4.049	−1.78009
	24.55	−1088.493308	4.150	−2.01113
	46.7	−1088.493341	4.203	−2.09778
	78.39	−1088.493357	4.215	−2.13978
PCM	4.9	−1088.509699	3.675	−45.0457
	10.36	−1088.513893	3.881	−56.0571
	24.55	−1088.516593	3.897	−63.1459
	46.7	−1088.517447	3.993	−65.3881
	78.39	−1088.518880	3.998	−69.1505

$\Delta E = E_{\text{Solvation}} - E_{\text{Gas}}$, ε = dielectric constant.

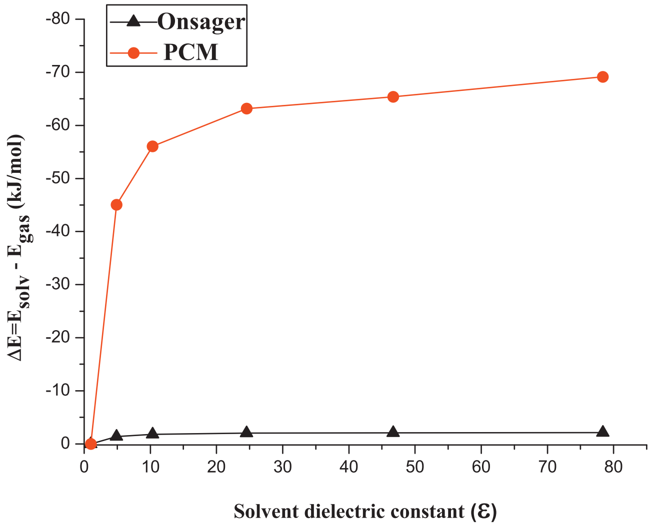

Fig. 5. Energy difference between the gas phase and solvent media by polarizable continuum model (PCM) and Onsager methods at B3LYP/6−31G(d) level of theory.

3.6. Atomic charge distributions in gas-phase and in solution-phase

The Mulliken atomic charges for the non-H atoms of (**I**) calculated at the B3LYP/6−31G(d) level in gas-phase are presented in Table 7. To investigate the solvent effect for the atomic charge distributions of (**I**), based on the B3LYP/6−31G(d) model and PCM method, three solvents (chloroform, ethanol and water) were selected and calculated values were also listed in Table 7. Mullikens atomic charge plot has shown in Fig. 6.

The Mulliken atomic charges show that the N1, N2 and N3 atoms of triazole ring, O1 atom of methoxy group and carbonyl O2 atom have larger negative atomic charges in the gas phase. This behavior may be the result of C10═O2 double bond character and electronegativity of triazole ring and methoxy group. On the other hand, it is found that, in solution-phase, the atomic charge values of the N2, N3 and O2 atoms are larger than those in gas-phase and while their atomic charge values will increase with the increase of the polarity of the solvent, that value of O1 and N1 decrease with the

Table 7
Atomic charges (e) of the title compound in gas phase and solution phase.

	In gas phase	In solution phase B3LYP/6−31G(d)		
	B3LYP/6−31G(d)	Chloroform (ε = 4.9)	Ethanol (ε = 24.55)	Water (ε = 78.39)
C1	0.373345	0.374088	0.374571	0.374671
C2	−0.028549	−0.021967	−0.019375	−0.018830
C3	−0.069672	−0.066861	−0.065786	−0.065600
C4	0.166487	0.165773	0.165393	0.165327
C5	−0.053238	−0.058844	−0.061174	−0.061636
C6	−0.058157	−0.060721	−0.061843	−0.062031
C7	0.262345	0.263004	0.263643	0.263777
C8	−0.031710	−0.032994	−0.033690	−0.033853
C9	0.194114	0.195728	0.196198	0.196278
C10	0.800928	0.801408	0.801480	0.801523
C11	0.542730	0.542808	0.542502	0.542483
C12	−0.111282	−0.106845	−0.105069	−0.104720
C13	0.187335	0.187326	0.187299	0.187308
C14	−0.042730	−0.043008	−0.043099	−0.043209
C15	0.000153	0.001088	0.001294	0.001359
C16	0.000941	0.002690	0.003410	0.003574
C17	−0.002467	−0.001510	−0.001071	−0.000978
C18	−0.035382	−0.036108	−0.036537	−0.036557
N1	−0.524079	−0.523677	−0.523536	−0.523520
N2	−0.141158	−0.146340	−0.147364	−0.147640
N3	−0.315725	−0.316532	−0.316754	−0.316811
O1	−0.505933	−0.502989	−0.501604	−0.501347
O2	−0.603430	−0.606152	−0.607883	−0.608143
O3	−0.004867	−0.009365	−0.011005	−0.011427

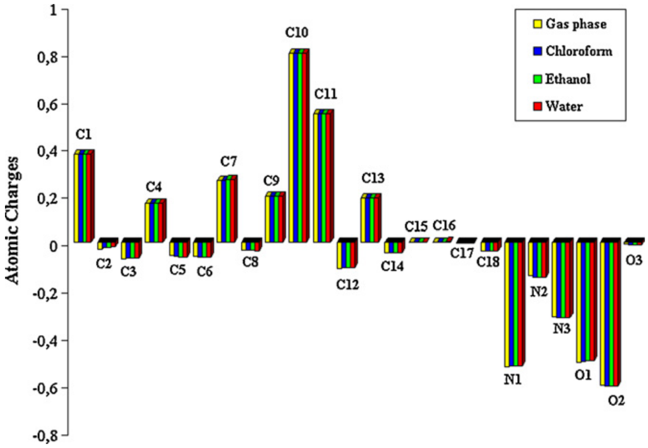

Fig. 6. Atomic charges of the title compound.

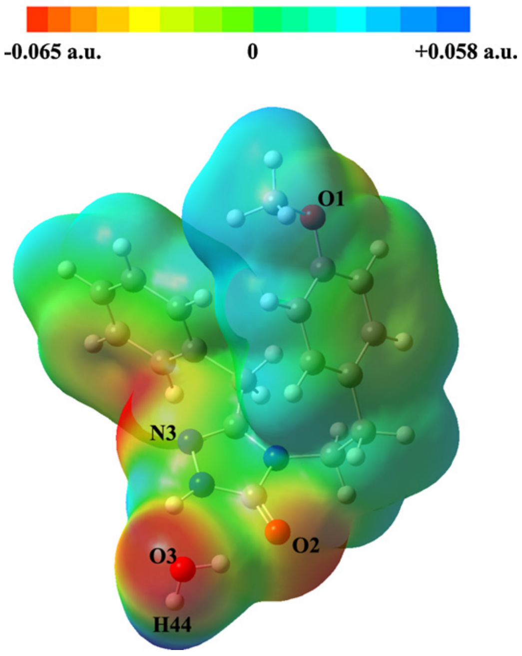

Fig. 7. Molecular electrostatic potential map calculated at B3LYP/6−31G(d) level. (For interpretation of the references to color in the text, the reader is referred to the web version of the article.)

increasing polarity of the solvent. The coordination of these atoms will changed in different solvents, which may be helpful when one wishes to use (**I**) to construct interesting metal complexes with different coordinate geometries [60]. This calculated result is not only consistent with many reported experimental values [61–63], it also supports the original idea of our synthesis.

3.7. Molecular electrostatic potential

The MEP is related to the electronic density and is a very useful descriptor for determining the sites for electrophilic and nucleophilic reactions as well as hydrogen bonding interactions [64]. The electrostatic potential $V(\mathbf{r})$ is also well suited for analyzing processes based on the “recognition” of one molecule by another, as in drug–receptor, and enzyme–substrate interactions, because it is through their potentials that the two species first “see” each other [65,66].

To predict reactive sites of electrophilic or nucleophilic attack for the investigated molecule, the MEP at the B3LYP/6−31G(d) optimized geometry was calculated. The negative (red and yellow) regions of the MEP are related to electrophilic reactivity and the positive (blue) regions to nucleophilic reactivity, as shown in Fig. 7. As can be seen from the figure, this molecule has several possible sites for electrophilic attack. Negative regions in the studied molecule were found around the carbonyl O2 atom, N3 atom of triazol ring and O1 atom. Also, a negative electrostatic potential region is observed around the O3 atom of water. The negative $V(\mathbf{r})$ values are −0.065 a.u. for O3 atom, which is the most negative region, −0.062 a.u. for N3 atom, −0.054 a.u. for O2 atom and −0.032 a.u. for O1 atom, which is a less negative region. However, a maximum positive region is localized on the H44 atom of the water with a value of +0.058 a.u. indicating a possible site for nucleophilic attack. According to these calculated results, the MEP map shows that the negative potential sites are on electronegative atoms as well as the positive potential sites are around the hydrogen atoms. These sites give information about the region from where the compound can have intermolecular interactions.

3.8. Natural bond orbital analysis

It is well-known that NBO analysis provides an efficient method for studying intra- and inter-molecular bonding and interaction among bonds, and also provides a convenient basis for investigating charge transfer or conjugative interaction in molecular systems [67]. The larger the $E^{(2)}$ value, the more intensive is the interaction between electron donors and electron acceptors, i.e., the more donating tendency from electron donors to electron acceptors and the greater the extent of conjugation of the whole system. Delocalization of electron density between occupied Lewis-type (bond or lone pair) NBO orbitals and formally unoccupied (antibond or Rydgberg) non-Lewis NBO orbitals correspond to a stabilizing donor–acceptor interaction.

In order to investigate the intermolecular interactions, the stabilization energies of (**I**) were computed by using second-order perturbation theory. For each donor NBO(i) and acceptor NBO(j),

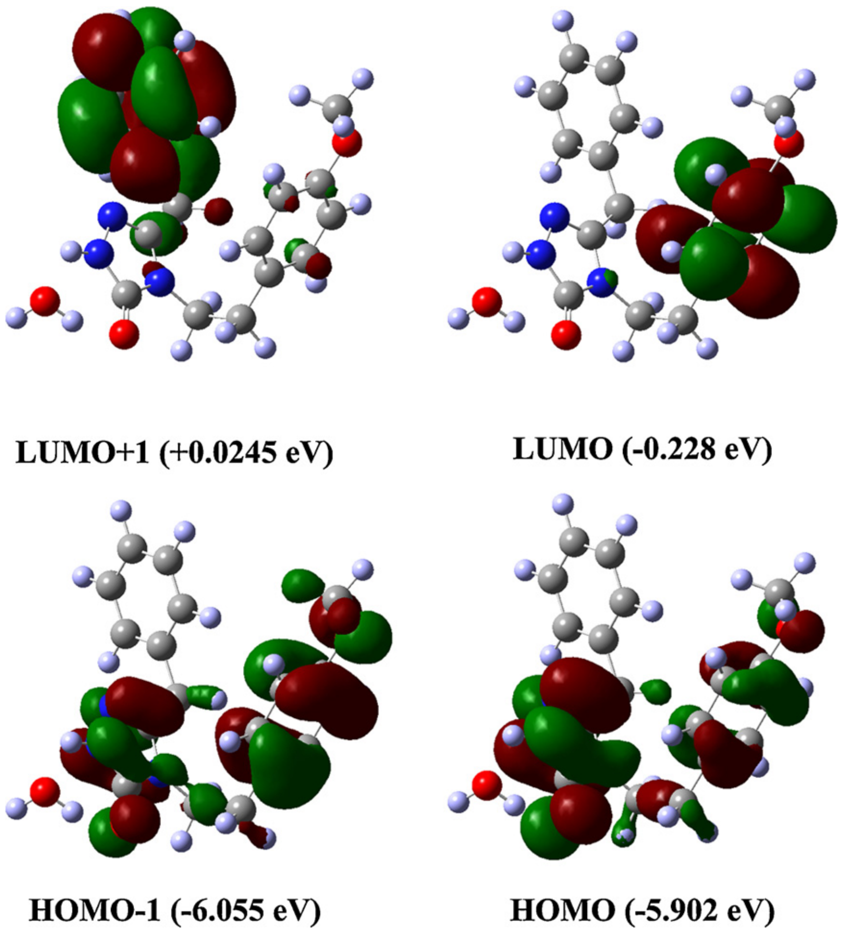

Fig. 8. Molecular orbital surfaces and energy levels given in parentheses for the HOMO−1, HOMO, LUMO and LUMO+1 of the title compound computed at B3LYP/6−31G(d) level.

Table 8
Second-order perturbation theory analysis of the Fock matrix in NBO basis, calculated at B3LYP/6−31G(d) level.

Donor orbital (i)	Acceptor orbital (j)	$E^{(2)}$ (kcal/mol)[a]	$\varepsilon_j - \varepsilon_i$ (a.u.)[b]	F_{ij}(a.u.)[c]
LP(1) O3	BD*(1) N2—H22	13.60	1.18	0.113
LP(1) O2	BD*(1) O3—H33	7.62	1.35	0.091
LP(2) O2	BD*(1) O3—H33	4.70	0.92	0.061
LP(3) O2	BD*(1) O3—H33	0.13	0.91	0.011
LP(1) O2	BD*(1) O3—H44	4.80	1.40	0.073
LP(2) O2	BD*(1) O3—H44	5.24	0.97	0.066

[a] $E^{(2)}$ means energy of hyper conjugative interactions.
[b] Energy difference between donor and acceptor i and j NBO orbitals.
[c] F_{ij} is the Fock matrix element between i and j NBO orbitals.

the stabilization energy $E^{(2)}$ associated with electron delocalization between donor and acceptor is estimated as [68,69]

$$E^{(2)} = -q_i \frac{(F_{ij})^2}{\varepsilon_j - \varepsilon_i} \tag{2}$$

where q_i is the donor orbital occupancy, ε_i, ε_j are diagonal elements (orbital energies) and F_{ij} is the off-diagonal NBO Fock matrix element. The results of second-order perturbation theory analysis of the Fock Matrix at B3LYP/6−31G(d) level of theory are presented in Table 8.

The NBO analysis has revealed that the $n(\mathrm{O3}) \rightarrow \sigma(\mathrm{N2{-}H22})$ interactions give the strongest stabilization to the system of (**I**) by 13.60 kcal/mol, and strengthen the intermolecular N2—H22···O3 hydrogen bond. We can say that the energy of the N2—H22···O3 hydrogen bond we obtained is reliable when it is compared with some values in literature. For example, Grabowski [70] has estimated the energy of the N—H···O hydrogen bond as 8.6 kcal/mol. Furthermore, the intermolecular H···O distance of the H22···O3 was observed to be 1.92(2) Å. This distance is significantly shorter than that of the van der Waals separation between O and H atoms (2.72 Å) [71]. This indicates the existence of the N2—H22···O3 intermolecular interaction for (**I**). There is another NBO interaction of the $n(\mathrm{O2}) \rightarrow \sigma(\mathrm{O3{-}H33})$ imply the existence of O3—H33···O2 hydrogen bond which has the total stabilization energy 12.45 kcal/mol. The lone pairs of O2 also donate its electrons to σ-type antibonding orbital for O3—H44. The total stabilization energy of O3—H44···O2 intermolecular hydrogen bonding is 10.04 kcal/mol. Thus, it is apparent that N—H···O and O—H···O interactions significantly influence crystal packing of this molecule.

3.9. *Frontier molecular orbitals*

The frontier molecular orbitals play an important role in the electric and optical properties, as well as in UV–vis spectra and chemical reactions [72]. Fig. 8 shows the distributions and energy levels of the HOMO−1, HOMO, LUMO and LUMO+1 orbitals computed at the B3LYP/6−31G(d) level for (**I**).

As seen from Fig. 8, both in the HOMO and HOMO−1, electrons are delocalized on the methoxyphenethyl fragment and triazole ring as well as O2 atom. For the LUMO, electrons are mainly delocalized on the methoxyphenethyl ring and for the LUMO+1 the electrons are delocalized on the benzyl ring. Both the highest occupied molecular orbitals (HOMOs) and the lowest-lying unoccupied molecular orbitals (LUMOs) are mainly localized on the rings, indicating that the HOMO–LUMO are mostly the π-antibonding type orbitals. The value of the energy separation between the HOMO and LUMO is 5.673 eV. This large HOMO–LUMO gap automatically means high excitation energies for many of excited states, a good stability and a high chemical hardness for (**I**).

3.10. Nonlinear optical effects

Nonlinear optical (NLO) effects arise from the interactions of electromagnetic fields in various media to produce new fields altered in phase, frequency, amplitude or other propagation characteristics from the incident fields [73]. NLO is at the forefront of current research because of its importance in providing the key functions of frequency shifting, optical modulation, optical switching, optical logic, and optical memory for the emerging technologies in areas such as telecommunications, signal processing, and optical interconnections [74–77].

The calculations of the total molecular dipole moment (μ), linear polarizability (α) and first-order hyperpolarizability (β) from the Gaussian output have been explained in detail previously [78], and DFT has been extensively used as an effective method to investigate the organic NLO materials.

It is well known that from the literature, the B3LYP approach provides fairly reliable values in electric hyperpolarizability calculations when compared with accuracies of traditional ab initio methods and this predictive capability of widely used B3LYP method is of interest to a wide audience of computational scientists [79,80]. In addition, taking into account reliability and the computational time required [28,81], the basis set 6−31+G(d) was chosen for the calculations of the hyperpolarizability in this study.

The electronic dipole moment $\mu_i (i = x, y, z)$, polarizability α_{ij} and the first hyperpolarizability β_{ijk} of (**I**) were calculated at the B3LYP/6−31+G(d) level using Gaussian 03W program package. Urea is one of the prototypical molecules used in the study of the NLO properties of molecular systems. Therefore it was used frequently as a threshold value for comparative purposes. The calculated values of α_{tot} and β_{tot} for (**I**) are, 335.218 Å^3 and 3.210×10^{-30} cm^5/esu, which are greater than those of urea (the α_{tot} and β_{tot} of urea are 4.890 Å^3 and 0.49×10^{-30} cm^5/esu obtained by B3LYP/6−31+G(d) method). When it is compared with the similar triazole compound in literature, the calculated value of β_{tot} of (**I**) is bigger than that of 4-(3-(1H-imidazol-1-yl)propyl)-5-methyl-2H-1,2,4-triazol-3(4H)-one monohydrate ($\beta_{\text{tot}} = 1.7506 \times 10^{-30}$ cm^5/esu calculated with B3LYP/6−31G(d) method) [14]. According to the magnitude of the first hyperpolarizability, (**I**) may be a potential applicant in the development of NLO materials.

To understand this phenomenon in the context of molecular orbital picture, we examined the molecular HOMOs and molecular LUMOs of (**I**) and showed in Fig. 8. The HOMO–LUMO energy gaps were calculated as 5.673 eV for (**I**), 6.35 eV for 4-(3-(1H-imidazol-1-yl)propyl)-5-methyl-2H-1,2,4-triazol-3(4H)-one monohydrate [14] and 6.891 eV for urea by B3LYP/6−31+G(d) method.

As can be seen from the β_{tot} values for these compounds, the larger value of first hyperpolarizability corresponds to the lower HOMO–LUMO gap. This correlation is following with the inverse relationship reported previously [82,83].

3.11. Thermodynamic properties

On the basis of vibrational analysis and statistical thermodynamics, the standard thermodynamic functions: heat capacity ($C^0_{p,m}$), entropy (S^0_m), and enthalpy (H^0_m) were obtained at B3LYP/6−31G(d) level and listed in Table 9.

Table 9
Thermodynamic properties at different temperatures at B3LYP/6−31G(d) level.

T (K)	H^0_m(kcal/mol)	$C^0_{p,m}$(cal/mol/K)	S^0_m(cal/mol/K)
250	11.421	76.648	157.832
298.15	15.525	89.830	172.810
300	15.695	90.333	173.380
350	20.647	103.660	188.620
400	26.246	116.191	203.555
450	32.447	127.695	218.150
500	39.196	138.109	232.361

Table 9 shows that the standard heat capacities, entropies, and enthalpies increase at any temperature from 250.00 to 500.00 K, because the intensities of molecular vibration increase with the increasing temperature. The correlation equations between these thermodynamic properties and temperature T are as follows:

$$C^0_{p,m} = -6.30835 + 0.37306\,T - 1.67959 \times 10^{-5} T^2 \quad (R^2 = 0.99993)$$

$$S^0_m = 74.99195 + 0.34783\,T - 6.61199 \times 10^{-5}\,T^2 \quad (R^2 = 1)$$

$$H^0_m = -0.9094 + 0.01816\,T + 1.24201 \times 10^{-4} T^2 \quad (R^2 = 0.99999)$$

These equations will be helpful for the further studies of (**I**).

4. Conclusions

4-(4-Methoxyphenethyl)-5-benzyl-2H-1,2,4-triazol-3(4H)-one monohydrate has been synthesized and characterized by FT-IR, NMR and X-ray single-crystal diffraction. The optimized geometrical parameters, vibrational frequencies, chemical shift values and some physicochemical properties have been calculated using the DFT/B3LYP method with 6−31G(d) basis set. The X-ray structure is found to be very slightly different from its optimized counterpart, and the crystal structure is stabilized by N—H···O and O—H···O hydrogen bonds. It was noted here that the experimental results belong to solid phase and theoretical calculations belong to gaseous phase. In the solid state, the existence of the crystal field along with the intermolecular interactions have connected the molecules together, which result in the differences of bond parameters between the calculated and experimental values. Despite the differences observed in the geometric parameters, the general agreement is good and the theoretical calculations support the solid-state structure. The vibrational frequencies and ^{1}H and ^{13}C NMR chemical shift values are precisely assigned to its molecular structure with the aid of the theoretical calculations at B3LYP/6−31G(d) level, in which the experimental and theoretical results support each other. The total energy of (**I**) decrease with the increasing polarity of the solvent and the stability of (**I**) increase in going from the gas phase to the solution phase. The nonlinear optical properties are also addressed theoretically. The predicted NLO properties of (**I**) are much greater than ones of urea. (**I**) is a good candidate as second-order NLO material. The MEP map shows that the negative potential sites are on electronegative atoms as well as the positive potential sites are around the hydrogen atoms. These sites give information about the region from where the compound can have intermolecular interactions. NBO analysis revealed that the $n(\text{O3}) \rightarrow \sigma(\text{N2—H22})$ interaction gives the strongest stabilization to the system, and the major interaction for the intermolecular O2···O3 contact is $n(\text{O2}) \rightarrow \sigma(\text{O3—H33})$. The correlations between the thermodynamic properties $C^0_{p,m}$, S^0_m, H^0_m and temperatures T are also obtained. We hope our paper will be helpful for the design and synthesis new materials.

Supplementary material

CCDC 796395 contains the supplementary crystallographic data for the compound reported in this paper. These data can be obtained free of charge at www.ccdc.cam.ac.uk/conts/retrieving.html [or from the Cambridge Crystallographic Data Centre (CCDC), 12 Union Road, Cambridge CB2 1EZ, UK; fax: +44 0 1223 336033; deposit@ccdc.cam.ac.uk].

References

[1] T. Tusukuda, Y. Shiratori, M. Watanabe, H. Ontsuka, K. Hattori, M. Shirai, N. Shimma, Bioorg. Med. Chem. Lett. 8 (1998) 1819–1824.
[2] J.T. Witkoaski, R.K. Robins, R.W. Sidwell, L.N. Simon, J. Med. Chem. 15 (1972) 1150–1154.
[3] G. Heubach, B. Sachse, H. Buerstell, Ger. Off. 2 (1979) 760–826.
[4] M. Kritsanida, A. Mouroutsou, P. Marakos, N. Pouli, S. Papakonstantinou-Garoufalias, C. Pannecouque, M. Witvrouw, E. De Clercq, Il Farmaco 57 (2002) 253–257.
[5] B.S. Holla, K.N. Poorjary, B.S. Rao, M.K. Shivananda, Eur. J. Med. Chem. 37 (2002) 511–522.
[6] M.I. Husain, M.J. Amir, Indian Chem. Soc. 63 (1986) 317–319.
[7] S.H.L. Chiu, S.E.W. Huskey, Drug Metab. Dispos. 26 (1998) 838–847.
[8] R. Eliott, R.L. Sunley, D.A. Griffin, UK Patent Appl. GB 2 (1986) 175–301.
[9] A.S. Lyakhov, A.N. Vorobiov, P.N. Gaponik, L.S. Ivashkevich, V.E. Matulis, O.A. Ivashkevich, Acta Crystallogr. C 59 (2003) o690–o693.
[10] H. Tanak, Y. Köysal, M. Yavuz, S. Isık, G. Gül, Acta Crystallogr. E 65 (2009) o3039.
[11] Y. Ünver, Y. Köysal, H. Tanak, D. Ünlüer, Ş. Işık, Acta Crystallogr. E 66 (2010) o1294.
[12] D.C. Sorescu, C.M. Bennett, D.L. Thompson, J. Phys. A 102 (1998) 10348–10357.
[13] A.A. El-Azhary, H.U. Suter, J. Kubelka, J. Phys. Chem. A 102 (1998) 620–629.
[14] H. Tanak, Y. Köysal, Y. Ünver, M. Yavuz, Ş. Işık, K. Sancak, Mol. Phys. 108 (2010) 127–139.
[15] F. Billes, H. Endredi, G. Keresztury, J. Mol. Struct. 530 (2000) 183–200.
[16] Y. Ünver, K. Sancak, H. Tanak, D. Değirmencioğlu, E. Düğdü, M. Er, S. Isık, J. Mol. Struct. 936 (2009) 46–55.
[17] S. Zaza, F. Guedira, S. Zaydoun, M. Saidi Idrissi, A. Lautie, F. Romain, Can. J. Anal. Sci. Spectrosc. 49 (2004) 15–23.
[18] M. Pagacz-Kostrzewa, R. Bronisz, M. Wierzejewska, Chem. Phys. Lett. 473 (2009) 238–246.
[19] P.J. Sanchez-Soto, E. Morillo, J.L. Perez-Rodriguez, C. Real, J. Therm. Anal. 45 (1995) 1189–1197.
[20] J. Li, T.A. Litzinger, Thermochim. Acta 454 (2007) 116–127.
[21] N.V. Kumar, U.C. Mashelkar, Heterocycl. Commun. 13 (2007) 211–214.
[22] O. Bekirarcan, H. Bektas, Molecules 11 (2006) 469–477.
[23] J.G. Haasnoot, Coord. Chem. Rev. 131 (2000) 200–202.
[24] W. Li, H.P. Jia, Z.F. Ju, J. Zhang, Cryst. Growth Des. 6 (2006) 2136–2140.
[25] P.J. van Koningsbruggen, Top. Curr. Chem. 233 (2004) 123–149.
[26] R. Bronisz, Inorg. Chem. 44 (2005) 4463–4465.
[27] F.D. Proft, P. Geerlings, Chem. Rev. 101 (2001) 1451–1464.
[28] H. Tanak, J. Phys. Chem. A (2011), doi:10.1021/jp205788b.
[29] H. Tanak, Int. J. Quantum Chem. (2011), doi:10.1002/qua.23206.
[30] H. Tanak, Comput. Theor. Chem. 967 (2011) 93–101.
[31] G. Fitzgerald, J. Andzelm, J. Phys. Chem. 95 (1991) 10531–10534.
[32] J. Andzelm, E. Wimmer, J. Chem. Phys. 96 (1992) 1280–1303.
[33] Stoe & Cie X-AREA (Version 1.18) X-RED32 (Version 1.04), Stoe&Cie, Darmstadt, Germany, 2002.
[34] G.M. Sheldrick, SHELXS97, SHELXL97, University of Gottingen, Germany, 1997.
[35] L.J. Farrugia, J. Appl. Crystallogr. 30 (1997) 565.
[36] H.B. Schlegel, J. Comput. Chem. 3 (1982) 214–218.
[37] C. Peng, P.Y. Ayala, H.B. Schlegel, M.J. Frisch, J. Comput. Chem. 17 (1996) 49–56.
[38] M.J. Frisch, G.W. Trucks, H.B. Schlegel, G.E. Scuseria, M.A. Robb, J.R. Cheeseman, J.A. Montgomery Jr., T. Vreven, K.N. Kudin, J.C. Burant, J.M. Millam, S.S. Iyengar, J. Tomasi, V. Barone, B. Mennucci, M. Cossi, G. Scalmani, N. Rega, G.A. Petersson, H. Nakatsuji, M. Hada, M. Ehara, K. Toyota, R. Fukuda, J. Hasegawa, M. Ishida, T. Nakajima, Y. Honda, O. Kitao, H. Nakai, M. Klene, X. Li, J.E. Knox, H.P. Hratchian, J.B. Cross, V. Bakken, C. Adamo, J. Jaramillo, R. Gomperts, R.E. Stratmann, O. Yazyev, A.J. Austin, R. Cammi, C. Pomelli, J.W. Ochterski, P.Y. Ayala, K. Morokuma, G.A. Voth, P. Salvador, J.J. Dannenberg, V.G. Zakrzewski, S. Dapprich, A.D. Daniels, M.C. Strain, O. Farkas, D.K. Malick, A.D. Rabuck, K. Raghavachari, J.B. Foresman, J.V. Ortiz, Q. Cui, A.G. Baboul, S. Clifford, J. ioslowski, B.B. Stefanov, G. Liu, A. Liashenko, P. Piskorz, I. Komaromi, R.L. Martin, D.J. Fox, T. Keith, M.A. Al-Laham, C.Y. Peng, A. Nanayakkara, M. Challacombe, P.M.W. Gill, B. Johnson, W. Chen, M.W. Wong, C. Gonzalez, J.A. Pople, Gaussian 03, Revision E.01, Gaussian, Inc., Wallingford, CT, 2004.
[39] J.B. Foresman, A. Frisch, Exploring Chemistry with Electronic Structure Methods, 2nd ed., Gaussian, Inc., Pittsburgh, 1996.
[40] R. Dennington II, T. Keith, J. Millam, GaussView, Version 4.1.2, Semichem, Inc., Shawnee Mission, KS, 2007.
[41] L. Onsager, J. Am. Chem. Soc. 58 (1936) 1486–1493.
[42] S. Miertus, E. Scrocco, J. Tomasi, Chem. Phys. 55 (1981) 117–129.
[43] V. Barone, M. Cossi, J. Phys. Chem. A 102 (1998) 1995–2001.
[44] M. Cossi, N. Rega, G. Scalmani, V. Barone, J. Comput. Chem. 24 (2003) 669–681.
[45] J. Tomasi, B. Mennucci, R. Cammi, Chem. Rev. 105 (2005) 2999–3093.
[46] P. Politzer, J.S. Murray, Theor. Chem. Acc. 108 (2002) 134–142.
[47] E.D. Glendening, J.K. Badenhoop, A.E. Reed, J.E. Carpenter, F. Weinhold, NBO. Version 3.1, Theoretical Chemistry Institute, University of Wisconsin, Madison, 1995.
[48] M. Hanif, G. Qadeer, N.H. Rama, J. Akhtar, M. Helliwell, Acta Crystallogr. E 65 (2009) o387.
[49] M. Hanif, G. Qadeer, N.H. Rama, W.-Y. Wong, Acta Crystallogr. E 64 (2008) o2180.
[50] H. Tanak, Y. Köysal, Y. Ünver, M. Yavuz, O. Büyükgüngör, K. Sancak, J. Mol. Model. 16 (2010) 447–457.
[51] A. Teimouri, A.N. Chermahini, K. Taban, H.A. Dabbagh, Spectrochim. Acta A 72 (2009) 369–377.
[52] R. Ustabaş, N. Süleymanoğlu, H. Tanak, Y.B. Alpaslan, Y. Ünver, K. Sancak, J. Mol. Struct. 984 (2010) 137–145.
[53] K. Sancak, Y. Ünver, H. Tanak, İ. Değirmencioğlu, E. Düğdü, M. Er, Ş. Işık, J. Inclusion Phenom. Macrocycl. Chem. 67 (2010) 325–334.
[54] T. Karakurt, M. Dinçer, A. Çukurovalı, İ. Yılmaz, J. Mol. Struct. 991 (2011) 186–201.
[55] M. Silverstein, G. Clayton Basseler, C. Morill, Spectrometric Identification of Organic Compounds, Wiley, New York, 1981.
[56] M. Ramalingam, V. Sethuraman, N. Sundaraganesan, Spectrochim. Acta A 78 (2011) 660–669.
[57] P.J. Garratt, in: A.R. Katritzky, C.W. Rees, E.F.V. Scriven (Eds.), Comprehensive Heterocyclic Chemistry II, vol. 4, Elsevier Science Ltd, 1996, pp. 127–163.
[58] A. Masternak, G. Wenska, J. Milecki, B. Skalski, S. Franzen, J. Phys. Chem. 109 (2005) 759–766.
[59] Y. Le, J.F. Chen, M. Pu, Int. J. Pharm. 358 (2008) 214–218.
[60] F.F. Jian, P.S. Zhao, Z.S. Bai, L. Zhang, Struct. Chem. 16 (2005) 635–639.
[61] M. Baldini, M. Belicchi-Ferrari, F. Bisceglie, G. Pelosi, S. Pinelli, P. Tarasconi, Inorg. Chem. 42 (2003) 2049–2055.
[62] L.J. Ashfield, A.R. Cowley, J.R. Dilworth, P.S. Donnelly, Inorg. Chem. 43 (2004) 4121–4123.
[63] J.S. Casas, E.E. Castellano, J. Ellena, M.S. Garcia Tasende, A. Sanchez, J. Sordo, M.J. Vidarte, Inorg. Chem. 42 (2003) 2584–2595.
[64] N. Okulik, A.H. Jubert, Internet Electron. J. Mol. Des. 4 (2005) 17–30.
[65] P. Politzer, P.R. Laurence, K. Jayasuriya, J. McKinney, Environ. Health Perspect. 61 (1985) 191–202.
[66] E. Scrocco, J. Tomasi, Topics in Current Chemistry, vol. 7, Springer, Berlin, 1973.
[67] M. Snehalatha, C. Ravikumar, I. Hubert Joe, N. Sekar, V.S. Jayakumar, Spectrochim. Acta A 72 (2009) 654–662.
[68] D.W. Schwenke, D.G. Truhlar, J. Chem. Phys. 82 (1985) 2418–2427.
[69] M. Gutowski, G. Chalasinski, J. Chem. Phys. 98 (1993) 4728–4738.
[70] S.J. Grabowski, J. Mol. Struct: Theochem. 811 (2007) 61–67.
[71] H. Sato, J. Dybal, R. Murakami, I. Noda, Y. Ozaki, J. Mol. Struct. 744 (2005) 35–46.
[72] I. Fleming, Frontier Orbitals and Organic Chemical Reactions, Wiley, London, 1976.
[73] Y.X. Sun, Q.L. Hao, W.X. Wei, Z.X. Yu, L.D. Lu, X. Wang, Y.S. Wang, J. Mol. Struct.: Theochem. 904 (2009) 74–82.
[74] C. Andraud, T. Brotin, C. Garcia, F. Pelle, P. Goldner, B. Bigot, A. Collet, J. Am. Chem. Soc. 116 (1994) 2094–2102.
[75] V.M. Geskin, C. Lambert, J.L. Bredas, J. Am. Chem. Soc. 125 (2003) 15651–15658.
[76] M. Nakano, H. Fujita, M. Takahata, K. Yamaguchi, J. Am. Chem. Soc. 124 (2002) 9648–9655.
[77] D. Sajan, H. Joe, V.S. Jayakumar, J. Zaleski, J. Mol. Struct. 785 (2006) 43–53.
[78] K.S. Thanthiriwatte, K.M. Nalin de Silva, J. Mol. Struct.: Theochem. 617 (2002) 169–175.
[79] G. Maroulis, D. Begue, C. Pouchan, J. Chem. Phys. 119 (2003) 794–798.
[80] G. Maroulis, J. Chem. Phys. 129 (2008) 044314–044321.
[81] C. Qin, Y. Si, G. Yang, Z. Su, Comput. Theor. Chem. 966 (2011) 14–19.
[82] M.C. Ruiz Delgado, V. Hernandez, J. Casado, J.T. Lopez Navarre, J.M. Raimundo, P. Blanchard, J. Roncali, J. Mol. Struct. 151 (2003) 651–653.
[83] J.P. Abraham, D. Sajan, V. Shettigar, S.M. Dharmaprakash, I. Nemec, I. Hubert Joe, V.S. Jayakumar, J. Mol. Struct. 917 (2009) 27–36.